Erbium in oxygen-doped silicon: Optical excitation

G. N. van den Hoven, Jung H. Shin, and A. Polman
FOM-Institute for Atomic and Molecular Physics, Kruislaan 407, 1098 SJ Amsterdam, The Netherlands

S. Lombardo and S. U. Campisano
Dipartimento di Fisica della Università Corso Italia, 57, I 95129 Catania, Italy

(Received 15 November 1994; accepted for publication 27 April 1995)

The photoluminescence of erbium-doped semi-insulating polycrystalline and amorphous silicon containing 30 at. % oxygen is studied. The films were deposited on single-crystal Si substrates by chemical vapor deposition, implanted with 500 keV Er to fluences ranging from 0.05 to 6×10^{15} ions/cm^2, and annealed at 300–1000 °C. Upon optical pumping near 500 nm, the samples show room-temperature luminescence around 1.54 μm due to intra-4f transitions in Er^{3+}, excited by photogenerated carriers. The strongest luminescence is obtained after 400 °C annealing. Two classes of Er^{3+} can be distinguished, characterized by luminescence lifetimes of 170 and 800 μs. The classes are attributed to Er^{3+} in Si-rich and in O-rich environments. Photoluminescence excitation spectroscopy on a sample with 1×10^{15} Er/cm^2 shows that ~2% of the implanted Er is optically active. No quenching of the Er luminescence efficiency is observed between 77 K and room temperature in this Si-based semiconductor. The internal quantum efficiency for the excitation of Er^{3+} via photogenerated carriers is 10^{-3} at room temperature. A model is presented which explains the luminescence data in terms of trapping of electrical carriers at localized Er-related defects, and subsequent energy transfer to Er^{3+} ions, which can then decay by emission of 1.5 μm photons. © *1995 American Institute of Physics.*

I. INTRODUCTION

One of the main problems faced in optoelectronic integration on silicon is the lack of an efficient silicon-based light source. This is because radiative band-to-band recombination in Si is not efficient due to the indirect band gap. An alternative way to achieve light emission is provided by optical doping. Trivalent rare-earth ions incorporated in solids can exhibit atomiclike optical transitions due to their incomplete 4f shell, shielded by filled 5s and 5p shells.[1] Although parity forbidden in the free ion, these intra-4f transitions are allowed in solids because of mixing of opposite parity states due to the presence of local electric fields in the solid host. This typically results in long lifetimes for some excited states, depending on the energy separation between the states and the phonon spectrum of the host material. Also, the local electric fields cause Stark splitting of the rare-earth energy levels. The rare-earth ion Er^{3+} is of interest[2,3] because of its $^4I_{13/2}\rightarrow{}^4I_{15/2}$ (first excited→ground state) transition around 1.54 μm, a wavelength within the telecommunications window of low loss silica-based optical fiber. Due to the absence of intermediate states between the $^4I_{13/2}$ and $^4I_{15/2}$ manifolds, the lifetime of the upper level can be in the order of milliseconds. Therefore, optical doping with Er is promising for devices such as optical amplifiers and lasers, where population inversion is a necessary requirement. The recombination energy of an electron–hole pair in Si is large enough to excite Er^{3+} to its first excited state through energy transfer, in principle enabling electrical excitation of the rare-earth ions in Si.

Optical doping of single-crystal silicon with Er has been extensively studied.[4–9] It has been found that very little Er^{3+} luminescence can be obtained in pure (float-zone grown, FZ) Si. Er-doped Czochralski-grown (Cz) Si shows enhanced Er^{3+} luminescence, due to the presence of ~10^{18} cm^{-3} oxygen.[7,8] Extended x-ray-absorption fine-structure (EXAFS) measurements reveal a local 4–6-fold coordination of O around Er in Cz Si.[10] A similar coordination is also found for Er in SiO_2.[11] Also, the low-temperature (4.4 K) photoluminescence spectra of Er^{3+} in Cz Si and in SiO_2 are rather similar, implying similar local surroundings for Er in these materials.[12] The maximum concentration of Er that can be optically activated in Cz Si is $\approx3\times10^{17}$ Er/cm^3.[13] Codoping of Si with additional O has been shown to improve the Er luminescence at room temperature by orders of magnitude, due to its effect of both increasing the optically active fraction of Er ions and reducing the temperature quenching.[14] Optically active Er concentrations as high as ~10^{18} cm^{-3} are needed for any useful applications.[15]

In this work, Er optical doping of semi-insulating polycrystalline and amorphous Si (SIPOS) is studied. SIPOS is deposited by chemical vapor deposition and consists of an amorphous Si matrix with a high (2–50 at. %) amount of O.[16–18] Annealing at around 900 °C leads to the formation of crystal Si nanograins (~5 nm diameter) surrounded by thin silicon oxide shells. SIPOS exhibits semiconducting properties depending on the O concentration.[16] The use of amorphous Si in combination with a high O concentration may allow for high concentrations of optically active Er, while circumventing the segregation[19,20] and precipitation[21] problems found in rare-earth doping of crystal Si. Our previous work on Er-implanted SIPOS has shown room-temperature photoluminescence at 1.54 μm.[22] Also, photoluminescence excitation spectroscopy showed that Er^{3+} in SIPOS can be excited via photocarriers generated by the pump light. In the present paper, it found that the Er^{3+} luminescence in SIPOS arises from two distinct classes of Er^{3+}. Only a very small temperature quenching of the luminescence is observed be-

 0021-8979/95/78(4)/2642/9/$6.00

tween 77 K and room temperature. Excitation spectroscopy shows that ~2% of the implanted Er is optically active. Internal quantum efficiencies for the excitation of Er^{3+} via photogenerated carriers are determined. The highest luminescence intensities are found for SIPOS with an amorphous microstructure containing high concentrations of both oxygen and hydrogen. The luminescence characteristics versus Er concentration and annealing temperature are also studied. In an accompanying paper[23] it is shown how room-temperature electroluminescence at 1.54 μm can be obtained from Er-doped SIPOS.

II. EXPERIMENT

SIPOS layers with a nominal O content of 30 at. % were formed by low-pressure chemical vapor deposition of SiH_4 and N_2O on to single-crystal (100) silicon substrates held at 620 °C. Following deposition, the films were implanted with 500 keV Er ions, with the samples held at room temperature. Er fluences ranged from 5×10^{13} to 6×10^{15} ions/cm^2. Postimplantation thermal annealing was performed at 300–1000 °C for 30 min in vacuum ($\approx5\times10^{-7}$ mbar). A number of films was preannealed at 920 °C for 30 min in O_2 before implantation in order to achieve the nanocrystalline microstructure mentioned above. A reference sample of 0.45 μm thick thermal SiO_2 on Si was implanted with Er to a total fluence of 1.9×10^{15} ions/cm^2 at several energies in order obtain a flat Er profile. This sample was subsequently annealed at 900 °C to attain optimum luminescence.[24]

SIPOS layer thickness and composition were measured by Rutherford backscattering spectrometry using 2 MeV $^4He^+$ and a scattering angle of 135°. The O concentration in the films was 31 at. %. Using an estimate of the density of SIPOS based on the volume fractions of Si and SiO_2, the SIPOS layer thickness was found to be 320–350 nm. The Er implantation profile peaked at ≈150 nm with a full width at half maximum of ≈90 nm. Er concentrations ranged from 0.008 to 1.0 at. %. Annealing above 800 °C caused the initially flat Si and O profiles to change near the surface, probably due to the formation of SiO_2. The Er profiles did not change upon annealing. Elastic recoil detection was performed in order to measure the H content of the films. As-implanted initially unannealed SIPOS showed a H concentration of ≈23 at. % throughout the layer. In the preannealed films the H concentration was around 0.3 at. %.

Photoluminescence (PL) spectroscopy was performed using a 48 cm single grating monochromator and a liquid–nitrogen-cooled Ge detector. The 514.5 nm line of an Ar ion laser was used as the excitation source. Pump powers ranged from 6 to 1500 mW, resulting in intensities of 1.2–300 W/cm^2 on the sample. For excitation spectroscopy a tunable Ti–sapphire laser (920 nm$<\lambda<$1030 nm) was employed at a power of 75 mW. The luminescence intensity was measured by mechanically chopping the excitation beam and monitoring the Ge detector signal using a lock-in amplifier. Luminescence decay measurements were performed by directly monitoring the Ge detector signal on an averaging digitizing oscilloscope system, after excitation with a pump pulse. The pulse length was varied between 50 μs and 30 ms. Measurements were performed either at room temperature in air or in a liquid–nitrogen cryostat, in which the temperature could be varied between 77 K and room temperature. Measurements at 15 K were performed using a closed cycle He refrigerator.

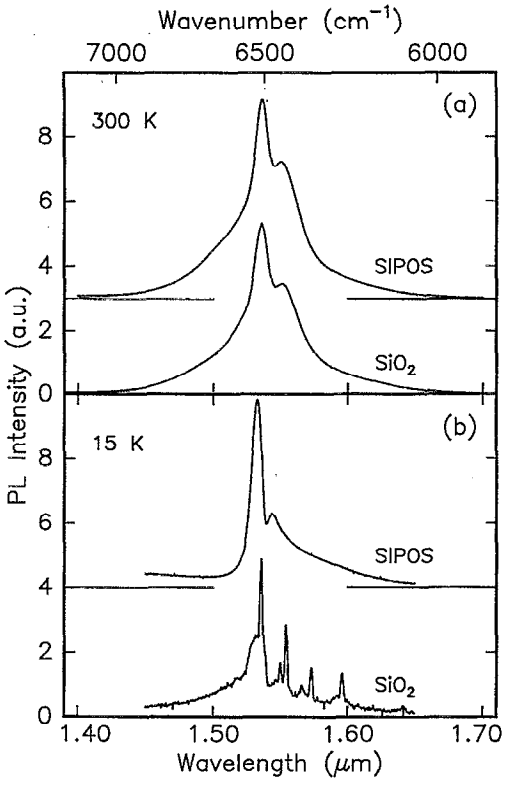

FIG. 1. PL spectra measured at (a) room temperature and at (b) 15 K for SIPOS with 31 at. % O. The initially unannealed SIPOS was implanted with 1×10^{15} 500 keV Er/cm^2 and then annealed at 400 °C. The spectra for an Er-implanted SiO_2 reference sample (1.9×10^{15} Er/cm^2) are shown on the same scale for comparison. The samples were pumped with 60 mW light at 514.5 nm.

III. RESULTS AND DISCUSSION

A. Site of Er^{3+}

Figure 1 shows the luminescence spectra for Er-implanted SIPOS and the SiO_2 reference sample obtained at room temperature and at 15 K. The (initially unannealed) SIPOS sample was implanted with 1×10^{15} Er/cm^2, and subsequently annealed at 400 °C. Both room-temperature spectra peak at 1.536 μm, and are typical of $^4I_{13/2}\rightarrow{}^4I_{15/2}$ transitions in Er^{3+}. Although the spectra are very similar at room temperature, those obtained at 15 K are markedly different: the spectrum for Er-implanted SiO_2 consists of a number of well-defined lines, whereas that of Er-implanted SIPOS shows a broad peak with a long shoulder toward longer wavelengths.

The sharp spectral features exhibited by Er^{3+} in SiO_2 are indicative of well-defined sites for the Er^{3+} ions. It may be that the covalent network of SiO_4 tetrahedra in the amorphous SiO_2 imposes structural constraints on the Er ions, resulting in a well-defined site for Er, as observed in EXAFS measurements.[11] For Er-implanted SIPOS, sharp spectral features are not observed, implying that the Er^{3+} ions may oc-

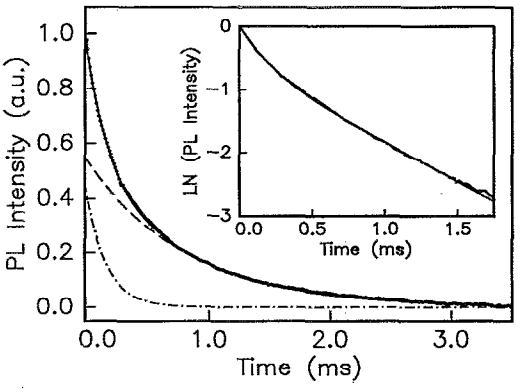

FIG. 2. Room-temperature photoluminescence decay at 1.536 μm of Er-implanted SIPOS (same sample as for Fig. 1) after pumping with a 20 ms, 514.5 nm pulse at 60 mW. The solid line is a double exponential fit to the data. The dashed–dotted and dashed lines are the two separate components of the double exponential decay.

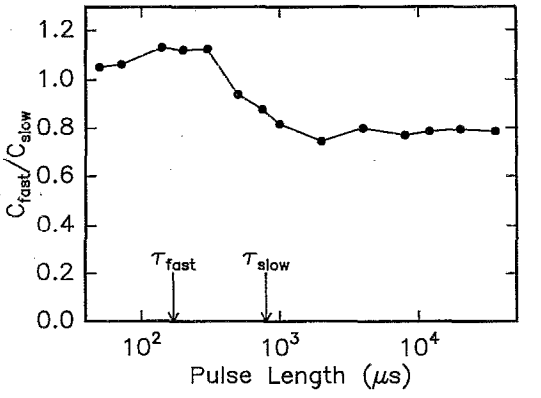

FIG. 3. Ratio C_{fast}/C_{slow} between the intensities of the fast and slow decaying component as a function of the length of the pump pulse for Er-implanted SIPOS. The fast (τ_{fast}) and slow (τ_{slow}) decay times are indicated in the figure. The pump power is 60 mW for all pulse durations. The sample is the same as for Fig. 1.

cupy a range of sites. Indeed, SIPOS is an amorphous mixture with a large range of bonding configurations, due to its nonstochiometric composition. As the temperature is increased, both SiO_2 and SIPOS spectra show homogeneous broadening due to interactions with phonons.

The Er^{3+} luminescence decay in SIPOS is shown in Fig. 2. The measurement was performed at room temperature on the same sample as above. The pump source was 60 mW of 514.5 nm laser light, chopped at 25 Hz, resulting in a block-shaped pump pulse of 20 ms. The luminescence signal at the peak of the spectrum ($\lambda = 1.536$ μm) was monitored. The decay may be fitted with two exponentials given by the equation

$$I_{PL}(t) = C_{fast} e^{t/\tau_{fast}} + C_{slow} e^{t/\tau_{slow}}, \quad (1)$$

where $I_{PL}(t)$ is the luminescence intensity as a function of time, τ_{fast} and τ_{slow} the lifetimes of the fast and slow decaying components, and C_{fast} and C_{slow} the prefactors of those decay components. A fit using Eq. (1) yields lifetimes of 164(2) and 806(4) μs for τ_{fast} and τ_{slow}, respectively, and a ratio C_{fast}/C_{slow} of 0.822(8). The decay curves deduced from the fit are shown in the figure. Note that fitting the data with three exponentials does not yield consistent results.

Two explanations may be given for the double exponential decay. First, one may assume two different "classes" of Er^{3+} in SIPOS, each with its characteristic decay time. Alternatively, the decay rate of a single class of excited Er^{3+} ions may depend on the degree of excitation, when processes such as cooperative upconversion[25] or energy migration followed by quenching play a role. This would result in non-single exponential decay as well. In order to distinguish between these possibilities, the ratio C_{fast}/C_{slow} between the luminescence intensities of the fast and slow decay channel was measured as a function of the pump pulse length.

Figure 3 shows the ratio C_{fast}/C_{slow} obtained by measuring the PL decay for pump pulses of different lengths. The pump power was 60 mW. In all cases the decay could be fitted with two exponentials, with the same two lifetimes as found above for Fig. 2. However, the ratio C_{fast}/C_{slow} did change with pulse length. The lifetimes τ_{fast} and τ_{slow} are indicated by arrows. C_{fast}/C_{slow} is found to change from ≈ 1.1 at short pulse lengths to ≈ 0.80 after very long pump pulses. The change occurs exactly between the decay times of 170 and 800 μs.

The observation that C_{fast}/C_{slow} decreases as the pulse length is increased rules out processes such as cooperative upconversion or energy migration followed by quenching. The rates of these processes increase with the degree of excitation of the Er^{3+} ions. This implies that for long pulses the fast decaying component would dominate, opposite to what is observed.

The observations of Fig. 3 may be understood by assuming two distinct classes of Er^{3+}, with characteristic lifetimes of $\tau_{fast} = 170$ μs and $\tau_{slow} = 800$ μs, each class corresponding to a set of similar sites having a narrow distribution of decay times. C_{fast}/C_{slow} is determined by the ratio between the population of excited Er^{3+} in the "fast class" and in the "slow class" at the moment that the pump pulse is switched off. After pumping with pulses much longer than the measured lifetimes, both populations have reached steady state, and C_{fast}/C_{slow} is independent of pulse length. For shorter pump pulses, on the order of τ_{slow}, the population of the slow decaying class has not reached steady state, and therefore C_{fast}/C_{slow} increases. For even shorter pulses, on the order of τ_{fast}, the fast decaying class also will not reach steady state. In the limit of infinitely short pulses, C_{fast}/C_{slow} will again be independent of pulse length, but it will now have a higher value than in the case of long pulses. The change in C_{fast}/C_{slow} measured in Fig. 3 is ~ 1.4. This value can also be calculated by solving the time dependent rate equations for the pump process, which include the pump rates and lifetimes of each class. Agreement with the data is found for pump rates of $\sim 10^4$ s^{-1}, a value consistent with the relatively high internal quantum efficiency measured in Sec. III C.

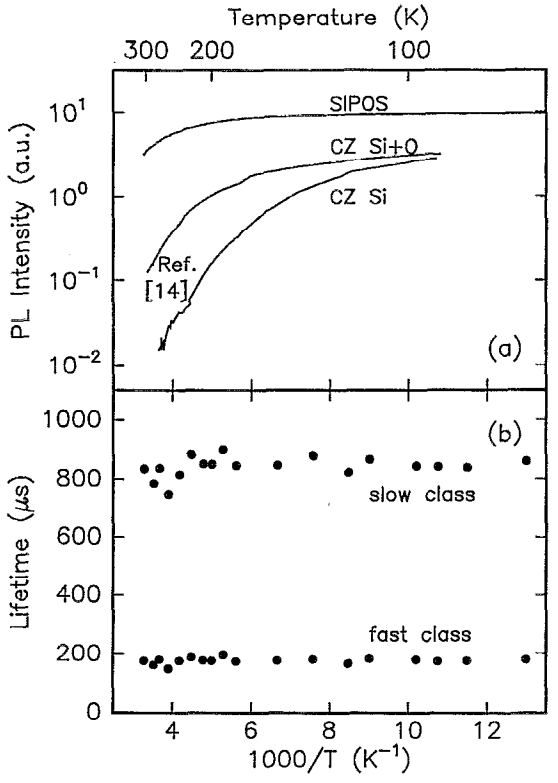

FIG. 4. (a) Arrhenius plot of the temperature dependencies of the 1.536 μm luminescence of Er-implanted initially unannealed SIPOS (same sample as for Fig. 1) and of Er-implanted Cz Si (9×10^{14} 250 keV Er/cm^2; annealed at 600 and 1000 °C) and Er-implanted Cz Si codoped with O (1.7×10^{15} Er/cm^2; 1×10^{19} O/cm^3) from Ref. 14 for comparison. The pump power was 60 mW in the case of SIPOS, and 200 mW in the case of Cz Si. (b) Luminescence lifetimes of the fast and slow decay classes of the Er-implanted SIPOS sample vs 1000/T.

B. Role of O

Figure 4 shows the temperature dependence of the Er^{3+} luminescence in SIPOS (initially unannealed; 1×10^{15} 500 keV Er/cm^2, annealed at 400 °C; same sample as for Fig. 1). The luminescence peak intensity, plotted in an Arrhenius fashion in Fig. 4(a), is found to decrease by a factor of 3 upon increasing the temperature from 77 to 300 K. Note that, although the spectral shape changes with temperature, the ratio between peak intensity and integrated intensity changes by less than 15% over the measured temperature range.

For comparison, the luminescence temperature dependence for Er-implanted Cz Si (9×10^{14} 250 keV Er/cm^2) and Er-implanted Cz Si (1.7×10^{15} Er/cm^2; concentration 1×10^{19} cm^{-3}) coimplanted with O (concentration 1×10^{20} cm^{-3}) taken from Ref. 14 are shown. For these samples, the luminescence intensity at low temperatures is a factor of 4 lower than that of Er-implanted SIPOS even though the pump power was more than 3× higher. Furthermore, the luminescence of Er in Cz Si decreases by two orders of magnitude when the temperature is increased to room temperature. Coimplanting with 1×10^{20} O/cm^3 results in a smaller decrease with increasing temperature. Figure 4(b) shows that the luminescence lifetimes τ_{fast} and τ_{slow} of Er in SIPOS are constant. The ratio C_{fast}/C_{slow} is also constant (not shown).

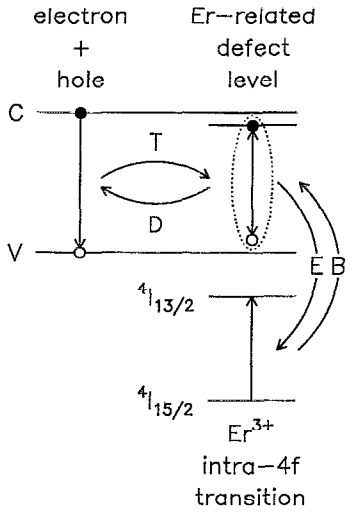

FIG. 5. Schematic of the excitation mechanism for Er^{3+} in Si. T and D indicate trapping and detrapping of electrical carriers at Er-related localized defect states. E indicates energy transfer to the Er^{3+} ions; B is backtransfer to the defect state. The Si conduction and valence band are indicated by C and V.

Figure 5 shows a schematic of a possible excitation mechanism for Er^{3+} in Si. An electron and a hole are trapped (T) at an Er-related defect. Subsequently, the carrier recombination energy is transferred to the Er^{3+}, which becomes excited (E) to the $^4I_{13/2}$ manifold. This excitation process may be efficient as the carriers are localized at the site of the Er^{3+} ion. In this scheme, backtransfer (B) of the Er^{3+} excitation to the defect state and detrapping (D) of electrical carriers from the defect may also occur. The rates of these processes depend on the energy mismatch between the different states, and therefore on the phonon density of states and temperature of the host material. In general, trapping and energy transfer to Er^{3+} are not or only weakly temperature dependent, as they occur through emission of phonons. In contrast, detrapping and backtransfer involve absorption of phonons, and so are temperature dependent. The localized Auger-type excitation mechanism sketched in Fig. 5 has been proposed earlier for rare earths in III–IV semiconductors, e.g., Yb in InP[26,27] and Er in GaAlAs.[28] In fact, the presence of a backtransfer process has been identified for Yb in InP.[29] An effective Hamiltonian for such excitation mechanisms has been derived for rare earths in semiconductors.[30] In the scheme of Fig. 5, the Er^{3+} luminescence intensity depends on:

(1) The pump efficiency, determined by the rates at which the electrical carriers are trapped and detrapped at the localized state, and by the rate of energy transfer to the Er^{3+} ion. The minority-carrier lifetime of the material determines the effective carrier concentration.

(2) The luminescence efficiency, defined as the ratio between radiative and total (radiative plus nonradiative) decay rates of the excited Er^{3+} ion. Backtransfer to the localized defect state is such a nonradiative decay channel, and will decrease the luminescence efficiency. Also, nonradiative energy transfer to non-Er-related defects may occur.

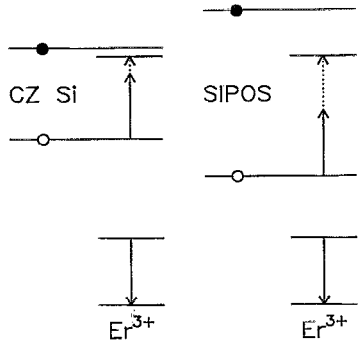

FIG. 6. Energy-level diagram including an Er-related localized defect state for Er in Cz Si, and Er in SIPOS. The arrows indicate deexcitation of Er^{3+} via backtransfer; the dotted arrows show the energy mismatch in this process.

(3) The amount of optically active Er, defined as all Er^{3+} whose $4f$ shell will be excited, and subsequently emit light through radiative decay.

Based on the above model, the data in Fig. 4 may be explained in a qualitative way. First, the PL intensities for Cz Si and SIPOS at 77 K will be compared. At this temperature the effect of backtransfer and detrapping is small, and the PL intensities are determined by the pump efficiency and Er^{3+} active concentration. For SIPOS, a higher PL intensity is observed than for Cz Si (with and without extra O), even though the electrical quality of (amorphous) SIPOS is much lower than that of Cz Si. The higher PL intensity from SIPOS is therefore attributed to a higher active Er^{3+} concentration and/or a higher excitation efficiency (T and E in Fig. 5). This will be discussed later on.

Second, the difference in quenching behavior for SIPOS and Cz Si is discussed. As the temperature is increased, three effects may take place: (1) the pump efficiency is reduced due to a decrease in carrier lifetime, (2) the Er^{3+} excitation efficiency may decrease due to enhanced detrapping, and (3) the luminescence efficiency may decrease, due to enhanced backtransfer, resulting in a lower luminescence lifetime for the Er^{3+}. Figure 4(b) shows that the luminescence lifetimes of the Er-implanted SIPOS sample are temperature independent, and therefore the luminescence efficiency is constant as a function of temperature. The small decrease in luminescence intensity with temperature for this sample is attributed to a small decrease in carrier lifetime or excitation efficiency (T, D, and E in Fig. 5). In contrast, it has been shown[14] that for Er-implanted Cz Si both the luminescence intensity and lifetime decrease with increasing temperature, giving evidence for a backtransfer process. In fact, in the O codoped sample the PL quenching is fully determined by backtransfer.

The results for SIPOS and Cz Si follow the trend that temperature quenching is reduced as the band gap of the host material is increased.[31,32] Increasing the band gap results in a larger energy mismatch between the states in Fig. 5, and so less backtransfer and/or deexcitation can take place. Comparing the band gap of SIPOS ($\approx$2 eV)[33] to that of Cz Si (1.1 eV) now explains why the temperature quenching is much lower in the SIPOS sample. Figure 6 shows this schematically. Both undoped and O codoped Cz Si have the same band gap, and indeed show similar backtransfer rates.[14] In the case of SIPOS, the band gap is so large that backtransfer and/or deexcitation become improbable, as a large number of phonons would be necessary to bridge the energy mismatch between the band-gap, Er-related defect state, and the Er^{3+} internal transition. As a consequence no quenching is observed.

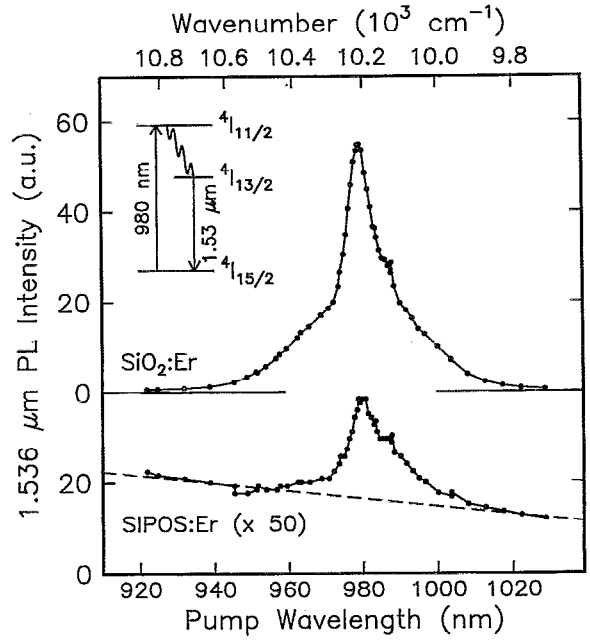

FIG. 7. Room-temperature photoluminescence excitation spectrum of Er-implanted SIPOS (1×10^{15} Er/cm^2, same sample as for Fig. 1) and of the Er-implanted SiO_2 reference sample (1.9×10^{15} Er/cm^2). The PL intensity at 1.536 μm is shown as a function of pump wavelength around 980 nm, for a constant pump power of 75 mW. The inset shows a schematic of the transitions involved.

Experiments have also been performed on Er-implanted preannealed SIPOS (annealed following implantation at 600 °C), containing the same amount of O but two orders of magnitude less H. In this case, temperature quenching of the luminescence lifetime and an accompanying decrease in PL intensity are observed (not shown), in contrast to the case for SIPOS that was initially unannealed (Fig. 4). This is probably a result of the presence of defects, such as unsaturated dangling bonds, acting as acceptors for the Er^{3+} excitation energy. Passivation of such defects using H would serve to reduce this nonradiative decay of the Er^{3+}.

C. Excitation of Er^{3+}

1. Er^{3+} optically active fraction

Figure 7 shows the room-temperature photoluminescence excitation spectra taken around 980 nm of Er-implanted SIPOS (initially unannealed; 1×10^{15} 500 keV Er/cm^2; annealed at 400 °C, as in Fig. 1), and of the SiO_2 reference sample. The pump wavelength was varied between 920 and 1030 nm, and the luminescence at 1.536 μm was monitored. The inset shows a schematic energy-level diagram of the transitions involved. Direct optical excitation of

Er^{3+} proceeds by absorption of a 980 nm pump photon, exciting the ion to the $^4I_{11/2}$ manifold. Subsequently, the ion decays to the first excited state ($^4I_{13/2}$), and then to the ground ($^4I_{15/2}$) state, emitting a photon around 1.54 μm. Varying the pump wavelength and monitoring the 1.536 μm luminescence reflects the structure of the $^4I_{11/2}$ absorption band. Such structures are observed for both the SiO_2 and SIPOS samples; however, in the case of SIPOS the spectrum rides on a background (indicated by the dashed line).

By solving the rate equation governing the pump process, the measured optically excited luminescence intensity around 1.54 μm may be written as:

$$I^{\text{opt}}=\frac{N^{\text{act}}}{\tau+1/R^{\text{opt}}}\,C^{\text{eff}},\quad \text{with } R^{\text{opt}}=\frac{I_{\text{pump}}\sigma_{\text{abs}}}{h\nu}, \tag{2}$$

where N^{act} is the areal density of optically active Er, τ the luminescence lifetime, R^{opt} the pump rate for optical excitation, $h\nu$ the pump photon energy, I_{pump} the pump intensity, σ_{abs} the absorption cross section for direct optical absorption of pump light by the Er^{3+}, and C^{eff} the collection efficiency of the setup. Note that the absorption coefficient of the SIPOS itself is small in this wavelength range.[33] Note also that Eq. (2) assumes only radiative decay from Er^{3+} in SIPOS, which is reasonable considering the independence of the luminescence lifetimes on temperature (Fig. 4). By comparing the measured luminescence intensities for SIPOS ($I^{\text{opt}}_{\text{SIPOS}}$) and SiO_2 ($I^{\text{opt}}_{\text{SiO}_2}$), and using Eq. (2) for both materials, N^{act} can now be estimated for SIPOS. Integrating the intensity of optically excited luminescence measured in Fig. 7 yields $I^{\text{opt}}_{\text{SIPOS}}/I^{\text{opt}}_{\text{SiO}_2}=6.5\times10^{-3}$. The absorption cross section of Er^{3+} in the SiO_2 reference sample was measured to be $\sigma_{\text{abs}}=7\times10^{-21}$ cm^2.[34] The Er luminescence lifetimes for the SIPOS and SiO_2 samples are $\approx$0.5 ms (weighted average of the fast and slow class) and 9.5 ms, respectively. The collection efficiencies were calculated by taking into account reflection and refraction at the interfaces of the samples. Assuming all of the Er in the SiO_2 reference sample is optically active ($N^{\text{act}}_{\text{SiO}_2}=1.9\times10^{15}$ cm^{-2}), and equal absorption cross sections for Er^{3+} in SIPOS and SiO_2, $N^{\text{act}}_{\text{SIPOS}}$ can then be calculated. This analysis yields $N^{\text{act}}_{\text{SIPOS}}=(2\pm1)\times10^{13}$ Er/cm^2; that is, (2±1)% of the implanted Er is optically active, corresponding to an optically active peak concentration of $\approx2\times10^{18}$ cm^{-3}. Note that this number is a lower limit due to the assumption that the decay of Er^{3+} in SIPOS is purely radiative. In any case, this number is an order of magnitude higher than the maximum concentration that can be activated in Cz Si (3×10^{17} cm^{-3}).[13] This confirms the suggestion made in Sec. III B, that the higher PL intensity at 77 K of Er-implanted SIPOS compared to Cz Si is due to more optically active Er in SIPOS.

2. Quantum efficiency

One can now also compare photocarrier mediated (electrical) luminescence in SIPOS, $I^{\text{el}}_{\text{SIPOS}}$, to optically excited luminescence in SiO_2, $I^{\text{opt}}_{\text{SiO}_2}$. Carrier mediated luminescence is only weakly dependent on pump wavelength in the range of Fig. 7, and the background of the SIPOS spectrum is partly due to such luminescence. Note that this background intensity is low compared to the direct optical-absorption component, due to the low optical-absorption coefficient of SIPOS around 980 nm. To enhance this component, measurements were done using 514.5 nm pump light: our previous work[22] has shown that at this wavelength Er in SIPOS is excited mainly through photogenerated carriers. The ratio $I^{\text{el}}_{\text{SIPOS}}/I^{\text{opt}}_{\text{SiO}_2}$ at 514.5 nm (45 mW, 6.3 W/cm^2) was found to be $\approx$7.6. The photocarrier mediated luminescence in SIPOS may be written as

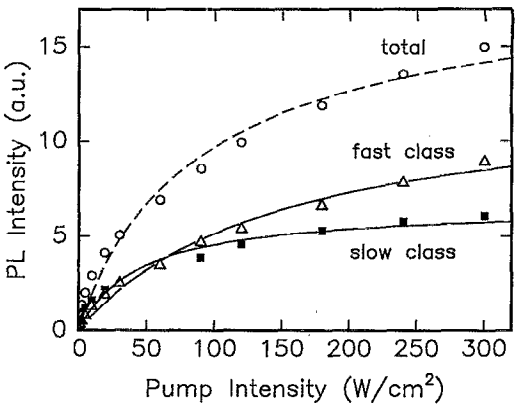

FIG. 8. Room-temperature 1.536 μm photoluminescence intensity of Er-implanted SIPOS (same sample as for Fig. 1) vs pump intensity. The open circles show the total PL intensity; the open triangles and solid squares show the separated contributions of each class of Er^{3+}. The solid lines are fits to the data according to Eq. (5), and give the population and quantum efficiency for each class. The dashed line is the sum of the fits, giving the total PL intensity.

$$I^{\text{el}}_{\text{SIPOS}}=\frac{N^{\text{act}}_{\text{SIPOS}}}{\tau_{\text{SIPOS}}+1/R^{\text{el}}}\,C^{\text{eff}}_{\text{SIPOS}}, \tag{3}$$

where R^{el} is the pump rate for excitation of Er^{3+} in SIPOS via photogenerated carriers. $I^{\text{opt}}_{\text{SiO}_2}$ is as in Eq. (2). Assuming that the active fraction of Er that can be excited optically ($N^{\text{act}}_{\text{SIPOS}}$ in Sec. III C 1) is the same as the fraction that can be excited via photocarriers, the only remaining free parameter in the ratio $I^{\text{el}}_{\text{SIPOS}}/I^{\text{opt}}_{\text{SiO}_2}$ is R^{el}, and can be determined: $R^{\text{el}}\approx145$ s^{-1} (at 6.3 W/cm^2 pump intensity).

The internal quantum efficiency (QE) for excitation of Er^{3+} via photocarriers can be defined as the fraction of photogenerated carriers which transfer their energy to Er^{3+}. As argued in Sec. III C 1, it can be assumed that the Er^{3+} emission is purely radiative, giving

$$\text{QE}=\frac{N^{\text{act}}_{\text{SIPOS}}R^{\text{el}}}{(1-\text{Refl})(1-e^{-\alpha D})\times I_{\text{pump}}/h\nu}, \tag{4}$$

where Refl is the reflection coefficient, α the optical-absorption coefficient of SIPOS at 514.5 nm,[33] and D the SIPOS layer thickness. Evaluating Eq. (4) yields the internal quantum efficiency for electrical excitation of Er^{3+} in SIPOS at room temperature: QE$\approx6\times10^{-4}$.

3. Inversion

Figure 8 (open circles) shows the luminescence intensity as a function of the pump intensity. The measurement was

performed at room temperature using the 514.5 nm line of an Ar laser as the pump source. The luminescence intensity is seen to increase sublinearly. At each pump intensity, decay traces were measured, as in Fig. 2. From the fits of the decay curves, C_{fast} and C_{slow} were determined; the lifetimes τ_{fast} and τ_{slow} were found to be constant within the error for all pump intensities. Subsequently, the intensity data were separated into the contributions of each class of Er^{3+} using the values for C_{fast} and C_{slow}. These results are shown as the open triangles and solid squares in Fig. 8. The slow class is observed to saturate at lower pump intensities than the fast class.

The observed saturation behavior can be explained in terms of excitation of all (optically active) Er^{3+} ions into the first excited state, i.e., inversion of the population. In steady state the PL intensity of each class is

$$I^{\text{PL}}_{\text{fast,slow}} \propto \frac{N^{\text{act}}_{\text{fast,slow}}}{\tau_{\text{fast,slow}} + 1/R^{\text{el}}_{\text{fast,slow}}}, \tag{5}$$

with the pump rate R^{el} proportional to the pump intensity as in Eq. (4), assuming the concentration of electrical carriers is proportional to the pump intensity. This is a good assumption for SIPOS in which unimolecular recombination dominates. Fits using Eq. (5) result in the solid lines shown in Fig. 8, and indicate that complete population inversion is nearly reached. The inversion sets in somewhat earlier in the case of the slow component, which is expected as its longer lifetime makes it easier to reach.

Evaluating the ratio between the PL intensities of each class in saturation, and using the fact that in saturation $I^{\text{PL}} \propto N^{\text{act}}/\tau$ [Eq. (5)], gives the optically active fluence in each class: $N^{\text{act}}_{\text{fast}} \approx 0.6\times10^{13}$ Er/cm^2, and $N^{\text{act}}_{\text{slow}} \approx 1.4\times10^{13}$ Er/cm^2. The corresponding internal quantum efficiencies per class are $\text{QE}_{\text{fast}} \approx 4\times10^{-4}$ and $\text{QE}_{\text{slow}} \approx 6\times10^{-4}$, giving a total of $\text{QE} \approx 1\times10^{-3}$, in agreement with the quantum efficiency determined in the previous section. Although the fits are good at high pump intensities, they deviate substantially from the data at low intensities. This may be due to energy transfer between the two classes of Er^{3+}.

D. Annealing behavior

The data on SIPOS shown so far were for initially unannealed material, implanted with Er to a fluence of 1×10^{15} cm^{-2}, and subsequently annealed at 400 °C. Initially unannealed SIPOS has an amorphous microstructure[17,18] and contains large amounts of H (~20 at. %). Annealing at 920 °C for 30 min in O_2 (here referred to as preanneal) results in phase separation of the material into a mixture of crystalline Si and SiO_2. Also, the H content is reduced by two orders of magnitude. Figure 9 shows luminescence data versus anneal temperature for both initially unannealed and preannealed SIPOS implanted with 1×10^{15} Er/cm^2. Annealing was done for 30 min in vacuum. Note that the Er implantation itself has amorphized any material which was initially crystalline.

The PL intensity, shown in Fig. 9(a), for initially unannealed SIPOS increases steeply up to its maximum at 400 °C, and then decreases again, sharply at first, up to 900 °C, where the luminescence is nearly undetectable. The

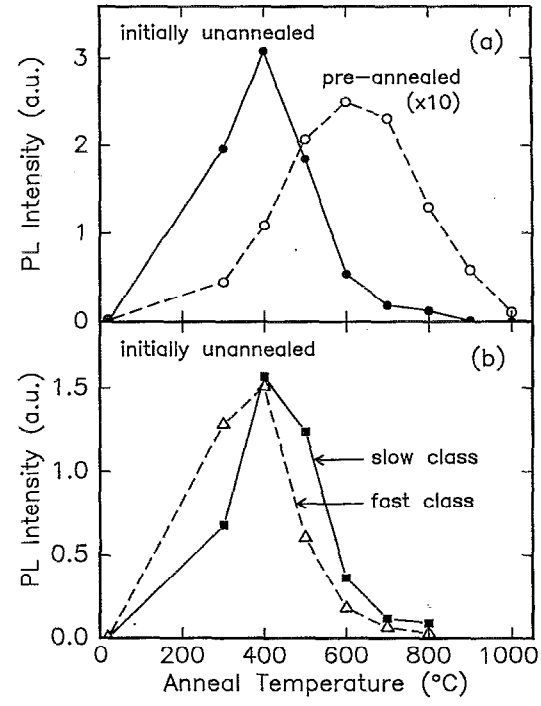

FIG. 9. Annealing behavior of the Er^{3+} luminescence of SIPOS implanted with 1×10^{15} 500 keV Er/cm^2. (a) Room-temperature luminescence peak intensities for initially unannealed and preannealed SIPOS. (b) Separated contributions of each class of Er^{3+} for initially unannealed SIPOS. All anneals were performed for 30 min in vacuum.

PL intensity for preannealed material shows a less steep increase, leading to a maximum luminescence signal after 600 °C annealing, one order of magnitude lower than for initially unannealed SIPOS. Annealing at higher temperatures also results in a decrease of the photoluminescence. A similar annealing behavior is observed for other Er fluences. Also, the electroluminescence intensity from Er-implanted SIPOS light emitting diodes[23] exhibits similar anneal characteristics (not shown).

The strong initial increase in PL intensity can be explained by three effects: (1) annealing reduces the number of defects which lower the carrier lifetime and act as nonradiative decay centers for Er^{3+}, (2) annealing might change the excitation probability and luminescence efficiency, and (3) annealing can incorporate Er on optically active sites. Ellipsometry data (not shown) indicate that the absorption coefficient of SIPOS is altered only slightly upon annealing. The fact that the absolute PL intensity of initially unannealed SIPOS is more than 10× higher than that of preannealed material is attributed to the difference in H content: the 920 °C preanneal reduces the H content by two orders of magnitude. It is well known that H passivates defects such as dangling bonds in amorphous Si, and can therefore increase the carrier lifetime in initially unannealed SIPOS, increasing the probability for carriers to excite Er^{3+}. Defect passivation will also reduce nonradiative quenching of the Er^{3+} transition. The intensity decrease above 400 °C for initially unannealed SIPOS may partly be due to out-diffusion of H, which is known to occur at this temperature.[35] Also, above 600 °C

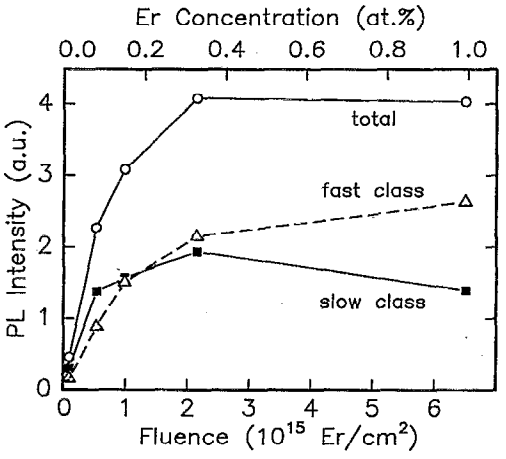

FIG. 10. Room-temperature 1.536 μm luminescence intensity vs Er fluence. The top scale shows the corresponding Er peak concentration. The samples were initially unannealed SIPOS implanted with 500 keV Er and annealed at 400 °C.

crystallization of SIPOS occurs, causing phase separation in the material. This may lead to a less favorable surrounding, or even precipitation of Er, and therefore a reduction in PL intensity.

In a similar way as in Fig. 8, the intensity data in Fig. 9(a) were separated into the contributions of the two classes of Er^{3+}. Figure 9(b) shows these data for initially unannealed (H containing, amorphous) SIPOS. Luminescence from the slow decay class dominates for high anneal temperatures, while the fast class is dominant for low-temperature anneals. These observations can be explained in terms of microstructural changes in the material. Upon increasing the anneal temperature, the random mixture of Si and O phase-separates into a mixture of Si and SiO_2. As Er in pure Si does not luminesce at room temperature, the remaining luminescent Er must be in a more SiO_2-like surrounding. At this stage one could postulate that the slow decaying Er^{3+} class resides in an O-rich surrounding, as it dominates at higher anneal temperatures. Indeed, the luminescence lifetime in SiO_2 (O rich)[24] is much higher than in Cz Si (O poor).[14] Consequently, the fast decay class arises from a Si-rich environment.

E. Er concentration dependence

Finally, the dependence of the luminescence intensity on Er fluence is shown in Fig. 10, for Er-implanted initially unannealed SIPOS, annealed at 400 °C. The corresponding Er peak concentration is shown on the top axis. The open circles show the total luminescence intensity, which increases up to an Er fluence of 2×10^{15}/cm^2 (0.15 at. %), and then levels off. The separate contributions of the two classes of Er^{3+} are also shown in Fig. 10. The relative contribution of the slow decaying class is larger at low concentrations, while above ~0.15 at. % the fast decaying class dominates. Following the same reasoning as above this implies that Si-rich Er^{3+} environments increase relative to the O-rich ones with increasing Er concentration. This implies that the maximum optically active Er concentration in SIPOS is limited by the O content.

IV. CONCLUSIONS

In conclusion, Er-implanted O-doped amorphous silicon exhibits room-temperature photoluminescence around 1.5 μm due to intra-4f transitions in Er^{3+}, excited via photogenerated electrical carriers. The luminescence arises from two distinct classes of Er^{3+}, characterized by luminescence lifetimes of 170 and 800 μs. The slow decay class may be related to Er^{3+} in an O-rich environment, while the fast decay class is attributed to Er^{3+} in a Si-rich surrounding. The intensities of each class depend in a different way on annealing temperature and Er concentration. Annealing at the optimum temperature of 400 °C results in defect annihilation, and an increase of the optically active Er concentration. H plays an important role in the passivation of defects which decrease the carrier lifetime and act as nonradiative decay centers for the Er^{3+}. Annealing above 400 °C causes H outdiffusion and crystallization of the material, resulting in less luminescence.

Despite its lower electrical quality, SIPOS exhibits stronger room-temperature Er photoluminescence than Cz Si. This is due to two effects: (1) there is no temperature quenching of the luminescence lifetime and (2) the optically active Er concentration is more than an order of magnitude higher. These effects are attributed to the high O and H content and amorphous nature of the material as well as the larger band gap. Er^{3+} is thought to be excited via trapping of an electron and a hole at an Er-related defect, and subsequent energy transfer to the Er^{3+} by recombination. Oxygen may form complexes with Er, which create such defect states in the band gap, thereby enabling efficient energy transfer to the Er^{3+} ions. Also, O may increase the amount of optically active Er. For initially unannealed SIPOS implanted with 1×10^{15} Er/cm^2 and then annealed at 400 °C, ~2% of the implanted Er is found to be optically active. The internal quantum efficiency is 10^{-3} at room temperature.

The main challenge now is to increase the optically active fraction of Er^{3+}. If all the Er is activated, an internal quantum efficiency in the 10% range may be possible.

ACKNOWLEDGMENTS

The authors would like to thank E. Snoeks, R. Serna, J. A. van der Elsken, F. W. Saris, S. Coffa (University of Catania), I. de Maat-Gersdorf (University of Amsterdam), and T. Gregorkiewicz (University of Amsterdam) for useful discussions. Work at the FOM-Institute was part of the research program of the Foundation for Fundamental Research on Matter (FOM), and was made possible by financial support from the Dutch Organization for the Advancement of Research (NWO), the IC Technology Program (IOP Electro-Optics) of the Ministry of Economic Affairs, and the Foundation for Technical Research (STW). Work at Catania University was partially supported by GNSM-CNR.

[1] S. Hüfner, *Optical Spectra of Transparent Rare-Earth Compounds* (Academic, New York, 1978).
[2] A. Polman, Mater. Res. Soc. Symp. Proc. **316**, 385 (1994).
[3] E. Desurvire, Phys. Today **47**, 20 (1994).
[4] H. Ennen, J. Schneider, G. Pomrenke, and A. Axmann, Appl. Phys. Lett. **43**, 943 (1983).
[5] H. Ennen, G. Pomrenke, A. Axmann, K. Eisele, W. Haydl, and J. Schneider, Appl. Phys. Lett. **46**, 381 (1985).
[6] Y. S. Tang, K. C. Heasman, W. P. Gillin, and B. J. Sealy, Appl. Phys. Lett. **55**, 432 (1989).
[7] P. N. Favennec, H. L'Haridon, D. Moutonnet, M. Salvi, and M. Gauneau, Jpn. J. Appl. Phys. **29**, 524 (1990).
[8] J. Michel, J. L. Benton, R. F. Ferrante, D. C. Jacobson, D. J. Eaglesham, E. A. Fitzgerald, Y.-H. Xie, J. M. Poate, and L. C. Kimerling, J. Appl. Phys. **70**, 2672 (1991).
[9] A. Polman, J. C. Custer, E. Snoeks, and G. N. van den Hoven, Nucl. Instrum. Methods B **80/81**, 653 (1993).
[10] D. L. Adler, D. C. Jacobson, D. J. Eaglesham, M. A. Marcus, J. L. Benton, J. M. Poate, and P. H. Citrin, Appl. Phys. Lett. **61**, 2181 (1992).
[11] M. A. Marcus and A. Polman, J. Non-Cryst. Solids **136**, 260 (1991).
[12] I. de Maat-Gersdorf, T. Gregorkiewicz, C. A. J. Ammerlaan, G. N. van den Hoven, and A. Polman (unpublished).
[13] A. Polman, G. N. van den Hoven, J. S. Custer, J. H. Shin, R. Serna, and P. Alkemade, J. Appl. Phys. **77**, 1256 (1995).
[14] S. Coffa, G. Franzò, F. Priolo, A. Polman, and R. Serna, Phys. Rev. B **49**, 16313 (1994).
[15] Y.-H. Xie, E. A. Fitzgerald, and Y. J. Mii, J. Appl. Phys. **70**, 3223 (1991).
[16] S. Lombardo, S. U. Campisano, and F. Baroetta, Phys. Rev. B **47**, 13561 (1993).
[17] P. Brüesch, Th. Stockmeier, and F. Stucki, J. Appl. Phys. **73**, 7677 (1993).
[18] M. Catalano, M. J. Kim, R. W. Carpenter, K. Das Chowdhury, and J. Wong, J. Mater. Res. **8**, 2893 (1993).
[19] A. Polman, J. S. Custer, E. Snoeks, and G. N. van den Hoven, Appl. Phys. Lett. **62**, 507 (1993).
[20] J. S. Custer, A. Polman, and H. M. van Pinxteren, J. Appl. Phys. **75**, 2809 (1994).
[21] D. J. Eaglesham, J. Michel, E. A. Fitzgerald, D. C. Jacobson, J. M. Poate, J. L. Benton, A. Polman, Y.-H. Xie, and L. C. Kimerling, Appl. Phys. Lett. **58**, 2797 (1991).
[22] S. Lombardo, S. U. Campisano, G. N. van den Hoven, A. Cacciato, and A. Polman, Appl. Phys. Lett. **63**, 1942 (1993).
[23] S. Lombardo, S. U. Campisano, G. N. van den Hoven, and A. Polman, J. Appl. Phys. **77**, 6504 (1995).
[24] A. Polman, D. C. Jacobson, D. J. Eaglesham, R. C. Kistler, and J. M. Poate, J. Appl. Phys. **70**, 3778 (1991).
[25] P. Blixt, J. Nilsson, T. Carlnäs, and B. Jaskorzynska, IEEE Photon. Technol. Lett. **3**, 996 (1991).
[26] K. Takahei, A. Taguchi, H. Nakagome, K. Uwai, and P. S. Whitney, J. Appl. Phys. **66**, 4941 (1989).
[27] A. Taguchi, H. Nakagome, and K. Takahei, J. Appl. Phys. **70**, 5604 (1991).
[28] T. Benyattou, D. Seghier, G. Guillot, R. Moncorge, P. Galtier, and M. N. Charasse, Appl. Phys. Lett. **58**, 2132 (1991).
[29] A. Taguchi, M. Taniguchi, and K. Takahei, Appl. Phys. Lett. **60**, 965 (1992).
[30] S. Schmitt-Rink, C. M. Varma, and A. F. J. Levi, Phys. Rev. Lett. **66**, 2782 (1991).
[31] P. N. Favennec, H. L'Haridon, D. Moutonnet, M. Salvi, and M. Gauneau, Mater. Res. Soc. Symp. Proc. **301**, 181 (1993).
[32] A. J. Neuhalfen and B. W. Wessels, Appl. Phys. Lett. **60**, 2657 (1992).
[33] G. Compagnini, S. Lombardo, R. Reitano, and S. U. Campisano, J. Mater. Res. **10**, 885 (1995).
[34] The absorption cross section (σ_{abs}) for the SiO_2 reference sample was obtained by measuring the pump rate (R^{opt}) at a given pump intensity.
[35] D. E. Carlson and C. W. Magee, Appl. Phys. Lett. **33**, 81 (1978).